Journal of Medicinal Chemistry

Article

pubs.acs.org/jmc

A Chemical–Biological Study Reveals C_9-type Iridoids as Novel Heat Shock Protein 90 (Hsp90) Inhibitors

Fabrizio Dal Piaz,[†] Antonio Vassallo,[‡] Abeer Temraz,[§] Roberta Cotugno,[†] Maria A. Belisario,[†] Giuseppe Bifulco,[†] Maria G. Chini,[†] Claudio Pisano,[⊥] Nunziatina De Tommasi,*[,†] and Alessandra Braca[∥]

[†]Dipartimento di Farmacia, Università di Salerno, Via Ponte Don Melillo, 84084 Fisciano (SA), Italy

[‡]Dipartimento di Scienze, Università degli Studi della Basilicata, Viale dell'Ateneo Lucano 10, 85100 Potenza, Italy

[§]Faculty of Pharmacy, Al Azhar University, Nasr-City, 11371 Cairo, Egypt

[⊥]Sigma-Tau Research and Development, Via Pontina Km 30,400, 00040 Pomezia (RM), Italy

[∥]Dipartimento di Farmacia, Università di Pisa, Via Bonanno 33, 56126 Pisa, Italy

Supporting Information

ABSTRACT: The potential of heat shock protein 90 (Hsp90) as a therapeutic target for numerous diseases has made the identification and optimization of novel Hsp90 inhibitors an emerging therapeutic strategy. A surface plasmon resonance (SPR) approach was adopted to screen some iridoids for their Hsp90 α binding capability. Twenty-four iridoid derivatives, including 13 new natural compounds, were isolated from the leaves of *Tabebuia argentea* and petioles of *Catalpa bignonioides*. Their structures were elucidated by NMR, electrospray ionization mass spectrometry, and chemical methods. By means of a panel of chemical and biological approaches, four iridoids were demonstrated to bind Hsp90 α. In particular, the dimeric iridoid argenteoside A was shown to efficiently inhibit the chaperone in biochemical and cellular assays. Our results disclose C_9-type iridoids as a novel class of Hsp90 inhibitors.

INTRODUCTION

Heat shock protein 90 (Hsp90) is an evolutionarily conserved abundant cytosolic chaperone (1–2% of cytosolic protein). It is involved in the turnover, trafficking, and activity of a large number and variety of "client" proteins, including apoptotic factors, protein kinases, transcription factors, signaling proteins, and a number of oncoproteins (ERK1/ERK2, survivin, EGFR, AKT, Raf-1, mutate p53).[1,2] Tumor cells require higher Hsp90 activity than normal cells to maintain their malignancy[3,4] since several oncoproteins are often mutated and/or overexpressed in these cells. Indeed, cancer cells can survive in stressed microenvironments by quickly selecting for adaptive mutations and chromosomal rearrangements that increase their survival abilities.[5,6] As a consequence, the efficiency of anticancer drugs that specifically target individual cancer promoting proteins may be gradually decreased, or even totally lost. One strategy to address this problem is to identify targets, such as Hsp90, proteasome, and autophagosome that affect multiple signaling pathways required for cancer cells to survive under stress.[7] Recent preclinical and clinical studies explored the effect of a combination of Hsp90 inhibitors and other anticancer agents in cancer therapy, and in most cases additives or synergic effects were observed.[8,9] These promising results further prompted the development of new anticancer drugs targeting Hsp90.

Thus, we adopted a surface plasmon resonance (SPR) assay to screen our natural compound libraries in order to find putative Hsp90 inhibitors. It is reasonable to expect that evolutionary pressures give plants producing secondary metabolites inhibitory to Hsp90 a competitive advantage, since such compounds may affect the growth and development of the insect pests and other pathogens.[10] Therefore, it was presumed that natural products represent a fertile territory for the identification of new Hsp90 inhibitors. Our libraries were developed selecting natural compounds with proven pharmacological activities, in areas such as apoptosis, cell cycle inhibition, and inflammation.[11] In the first step of our target-oriented screening some scaffolds were selected such as kaurane-type diterpenes, germacrane-like sesquiterpenes, limonoids, and iridoids.[12,13] Among iridoids, secoiridoids (secologanin, sweroside), iridoids (loganin, geniposide, adenosmoside), and a C_9-type iridoid (verminoside) were screened; only the latter showed promising inhibitory activity toward Hsp90. These results motivated the phytochemical investigation of plants belonging to Bignoniaceae family, well-known for their C_9-type iridoid content. Our phytochemical studies led to the isolation of 8 iridoids (**1**–**8**) from *Tabebuia argentea* Britt., including 2 new unusual dimers (**1**–**2**), and 16 iridoids (**9**–**24**) from *Catalpa bignonioides* Walter, 11 of which (**9**–**19**) were new compounds. Structural identification was

Received: September 26, 2012
Published: January 30, 2013

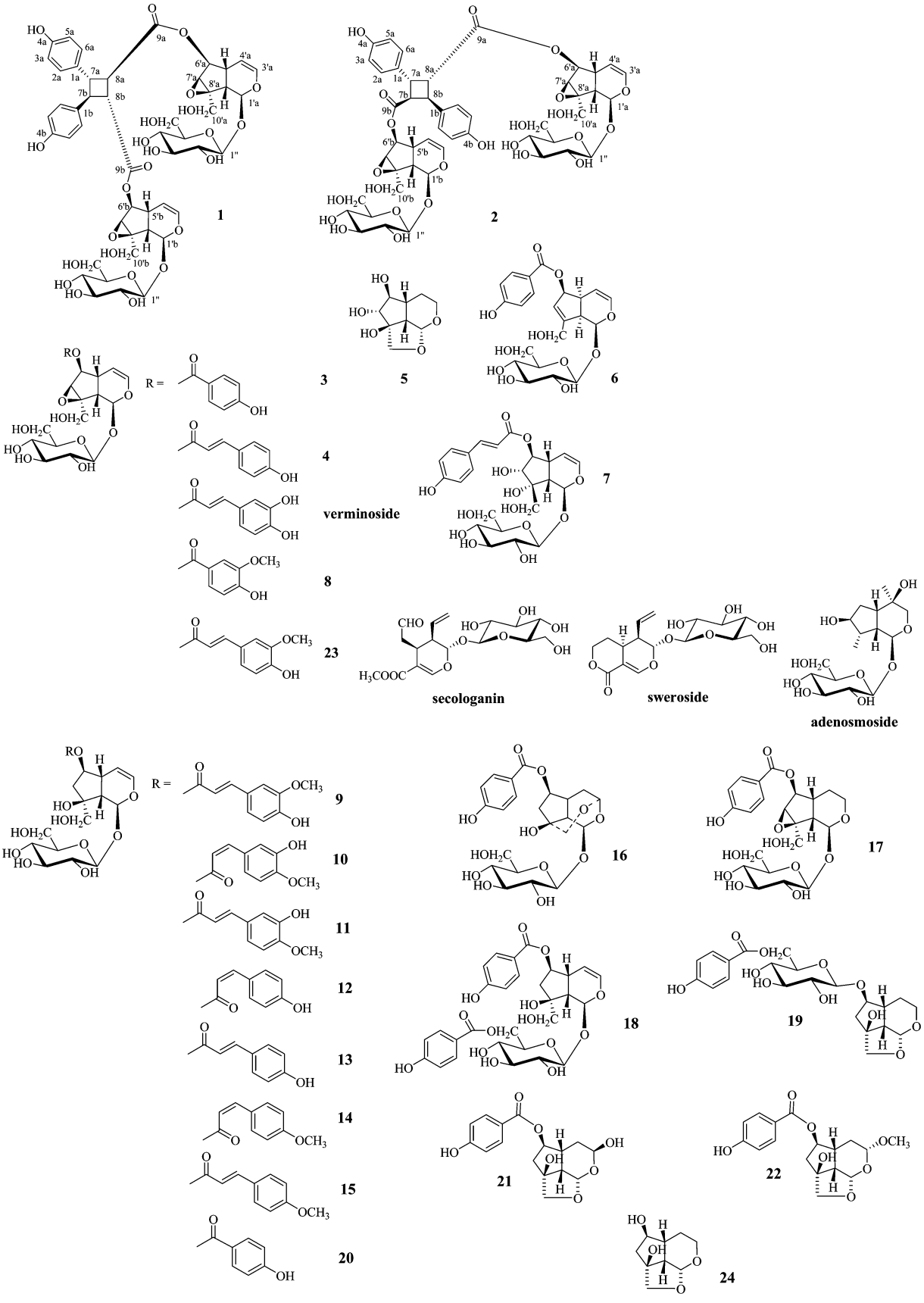

Figure 1. Structures of iridoids.

conducted by analysis of one- and two-dimensional (1D and 2D) NMR spectroscopic and mass spectrometry data.

Herein we report the evaluation of the Hsp90 inhibitory activity of compounds **1**−**24** by means of a panel of chemical and

dx.doi.org/10.1021/jm301398y | J. Med. Chem. 2013, 56, 1583−1595

biological approaches, including SPR measurements, biochemical and cellular assays, limited proteolysis, and molecular docking. Four iridoids, particularly the dimer **1**, were shown to bind Hsp90 inhibiting its ATPase activity. Our results disclose C_9-type iridoids as a novel class of Hsp90 inhibitors.

RESULTS AND DISCUSSION

Iridoid Isolation and Structure Elucidation. The leaves of *T. argentea* and the petioles of *C. bignonioides* were extracted with solvents of increasing polarity. After separation by Sephadex LH-20, the reverse phase HPLC was employed to obtain the purified iridoids. Compounds **1**−**8** were isolated from *T. argentea*, while compounds **9**−**24** were obtained from *C. bignonioides* (Figure 1).

The molecular formula of compound **1** was determined as $C_{48}H_{56}O_{24}$ by high-resolution electrospray ionization mass spectrometry (HRESIMS) spectrum showing a quasi-molecular ion peak at *m/z* 1039.3186 $[M + Na]^+$ in the positive ion mode. The ^{1}H NMR spectrum of **1** (Table 1) was very similar to that of the iridoid specioside (**4**),[14] the only point of difference being the absence of the *trans* olefinic protons of the cinnamoyl moiety. This data, in combination with the molecular weight which was exactly twice that of **4**, clearly indicated **1** as a dimer of **4**. This is a characteristic of the cyclobutane-type dimers, where the double bonds of the dimerized subunits are involved in the formation of a cyclobutane ring.[15,16] The type of dimerization of **1** can be easily deduced by MS/MS analyses.[17] Indeed, if a *head-to-tail* dimer undergoes collision-induced dissociation (CID) fragmentation, any event involving the cyclobutane ring would produce two identical species with a molecular weight of 508.2; otherwise, in the case of a *head-to-head* dimer two different pairs of monomer fragments would be produced: a symmetric breakdown of the cyclobutane ring would generate two identical monomers (M_r 508.2), whereas an asymmetric fragmentation would produce a "light" monomer characterized by both the phenolic moieties (M_r 212.1) and a "heavy" monomer presenting both the iridoidic groups (M_r 804.2). In the case of compound **1**, the ESIMS/MS spectrum acquired in the negative ion mode showed three diagnostic species at *m/z* 803, 507, and 211, thus indicating a *head-to-head* dimerization for **1**. In the ^{1}H NMR spectrum of **1** the cyclobutane protons could be clearly observed as two doublets at δ 3.97 and 4.23 (d, J = 6.0 Hz) correlating with signals at 44.4 and 45.9 ppm in the HSQC spectrum. Signals ascribable to two units of iridoid glucosides were also present. Assignments of all chemical shifts of protons and carbons were established from a combination of 1D-TOCSY, DQF-COSY, and HSQC analyses. The heteronuclear multiple bond correlation (HMBC) experiment of **1** indicated connections between H-7a—C-2a, H-7a—C-9a, H-8a—C-1a, H-8a—C-8b, H-7b—C-2b, H-7b—C-9b, H-8b—C-8a, H-8b—C-1b, H-8b—C-9b, H-1′—C-1″. Therefore, the acid moiety of this dimer should possess the truxinic acid skeleton.[16] In order to determine the relative configuration of compound **1**, we considered both the MS data and the possible combinations of the parent compound **4**. Compound **1** derived from a *head-to-head* condensation (Figure 2) that may provide the two different stereoisomers **1a** and **1b**. Analysis of the minimum energy conformers for the two possible combinations (**1a** and **1b**) revealed that experimental NOE's for **1** was in accordance only with stereoisomer **1a** (Figure 3), in particular, the correlations between H-8a and H-7a, and H-8a and H-6a/H-2a. Moreover, such findings were in accordance with the experimental evidence

Table 1. ^{1}H and ^{13}C NMR Data of Compounds 1 and 2 (CD_3OD, 600 MHz)[a]

	1		2	
position	δ_H	δ_C	δ_H	δ_C
1a, 1b		130.6		130.8
2a, 2b	6.84 d (8.5)	130.5	7.21 d (8.0)	129.7
3a, 3b	6.56 d (8.5)	115.7	6.75 d (8.0)	116.2
4a, 4b		156.2		157.9
5a, 5b	6.56 d (8.5)	115.7	6.75 d (8.0)	116.2
6a, 6b	6.84 d (8.5)	130.5	7.21 d (8.0)	129.7
7a	4.23 d (6.0)	45.9	4.45 dd (10.0, 9.0)	41.8
7b	4.23 d (6.0)	45.9	4.37 dd (10.0, 9.0)	41.8
8a	3.97 d (6.0)	44.4	3.97 dd (10.0, 9.0)	48.3
8b	3.97 d (6.0)	44.4	4.05 dd (10.0, 9.0)	48.0
9a		174.3		174.0
9b		174.3		173.6
1′a	5.15 d (4.5)	94.8	4.99 d (4.5)	94.7
1′b	5.15 d (4.5)	94.8	5.02 d (4.5)	94.7
3′a	6.36 dd (6.0, 2.0)	142.2	6.17 dd (6.0, 2.0)	141.3
3′b	6.36 dd (6.0, 2.0)	142.2	6.25 dd (6.0, 2.0)	141.7
4′a	5.07 dd (6.0, 3.5)	102.7	4.16 dd (6.0, 3.5)	103.1
4′b	4.97 dd (6.0, 3.5)	102.7	4.67 dd (6.0, 3.5)	102.7
5′a	2.55 m	36.2	2.15 m	36.2
5′b	2.55 m	36.2	2.33 m	36.0
6′a	5.08 dd (6.0, 5.5)	82.7	4.61 dd (6.0, 5.5)	81.4
6′b	5.01 dd (6.0, 5.5)	82.7	4.72 dd (6.0, 5.5)	80.6
7′a, 7′b	3.72 d (5.5)	60.0	3.86 d (5.5)	56.4
8′a, 8′b		67.0		66.0
9′a	2.59 dd (9.5, 4.5)	42.8	2.48 dd (9.5, 4.5)	42.6
9′b	2.59 dd (9.5, 4.5)	42.8	2.53 dd (9.5, 4.5)	42.6
10′a	3.83 d (12.0)	61.3	3.68 d (12.0)	61.1
10′b	4.15 d (12.0)		4.08 d (12.0)	
Glc 1″a,1″b	4.77 d (8.0)	99.4	4.73 d (8.0)	99.4
2″a, 2″b	3.23 dd (9.5, 8.0)	74.8	3.23 dd (9.5, 8.0)	74.6
3″a, 3″b	3.41 t (9.5)	77.4	3.39 t (9.5)	77.3
4″a, 4″b	3.27 t (9.5)	71.4	3.20 t (9.5)	71.6
5″a, 5″b	3.34 m	78.2	3.27 m	77.6
6″a, 6″b	3.66 dd (12.0, 4.5)	62.8	3.59 dd (12.0, 4.5)	62.6
	3.93 dd (12.0, 3.0)		3.89 dd (12.0, 3.0)	

[a] J values are in parentheses and reported in Hz; chemical shifts are given in ppm; assignments were confirmed by DQF-COSY, 1D-TOCSY, HSQC, and HMBC experiments.

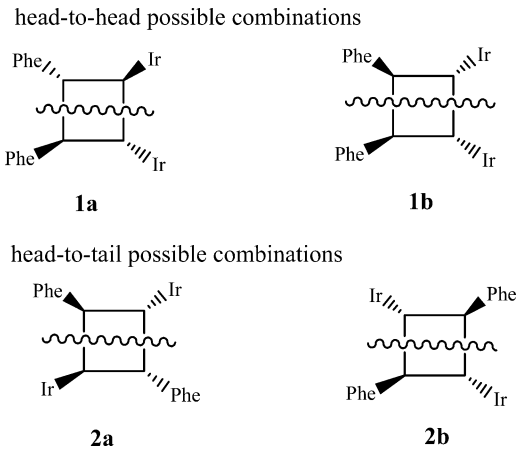

Figure 2. Possible combination of argenteoside A (**1**) and B (**2**) dimerization.

dx.doi.org/10.1021/jm301398y | J. Med. Chem. 2013, 56, 1583−1595

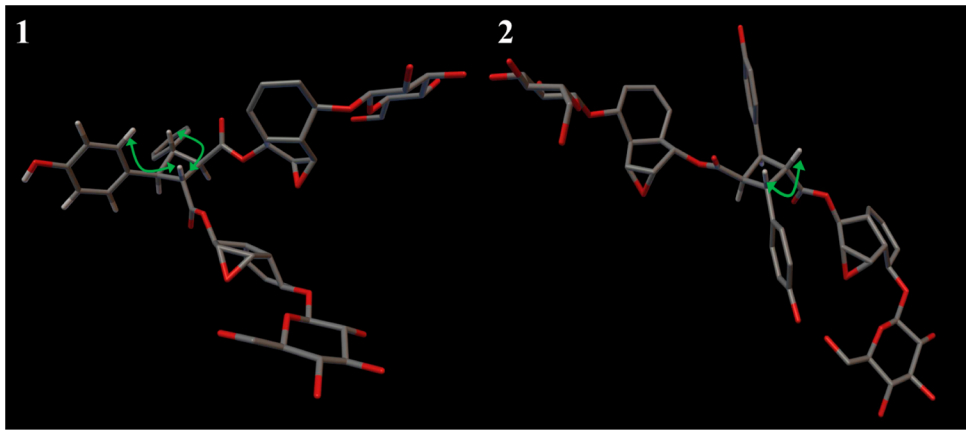

Figure 3. Crucial NOE correlations of argenteoside A (**1**) and B (**2**).

Table 2. ^{1}H and ^{13}C NMR Data of Compounds 9−15 (CD_3OD, 600 MHz)[a]

	9		10/11		12/13		14/15	
position	δ_H	δ_C	δ_H	δ_C	δ_H	δ_C	δ_H	δ_C
1	5.57 d (4.0)	93.0	5.55 d (4.2)	92.9	5.54 d (5.0)	93.0	5.55 d (4.0)	92.8
3	6.27 dd (6.0, 1.5)	141.5	6.28 dd (6.0, 2.5)	141.3	6.27 dd (6.0, 3.0)	141.1	6.29 dd (6.0, 2.5)	141.4
4	4.99 dd (6.0, 4.0)	104.2	5.00 dd (6.5, 3.5)	104.0	5.00 dd (6.0, 3.5)	103.9	5.02 dd (6.0, 3.0)	103.0
5	3.03 m	40.3	3.01 m	40.2	2.99 m	40.3	3.00 m	40.2
6	4.98 m	80.4	4.98 m		5.04 m		5.08 m	80.5
7a	1.96 br d (7.5)	42.3	1.87 br d (7.5)	42.2	1.88 dd (14.5, 2.5)	42.6	1.81 dd (14.0, 2.5)	42.5
7b	2.32 dd (15.0, 6.5)		2.36 dd (14.5, 6.0)		2.37 dd (14.5, 6.0)		2.35 dd (14.0, 6.0)	
8		82.7		82.5		82.7		82.5
9	2.59 dd (9.0, 4.0)	51.5	2.56 dd (9.0, 4.0)	51.1	2.58 dd (8.0, 4.0)	51.1	2.57 dd (8.5, 4.5)	51.2
10a	3.61 d (12.0)	67.7	3.61 d (11.5)	67.7	3.61 d (12.0)	67.5	3.64 d (11.5)	67.7
10b			3.72 d (11.5)		3.72 d (12.0)		3.75 d (11.5)	
Glc 1′	4.68 d (7.8)	99.4	4.67 d (7.8)	99.2	4.66 d (7.8)	99.0	4.68 d (7.8)	99.3
2′	3.20 dd (9.0, 7.8)	74.6	3.18 dd (9.0, 7.8)	74.6	3.20 dd (9.5, 7.8)	74.5	3.21 dd (9.0, 7.8)	74.4
3′	3.29 t (9.0)	78.1	3.29 t (9.0)	78.0	3.28 t (9.5)	78.1	3.43 t (9.0)	78.2
4′	3.26 t (9.0)	71.2	3.22 t (9.0)	71.2	3.21 t (9.5)	70.8	3.32 t (9.0)	71.0
5′	3.38 m	77.7	3.39 m	77.6	3.39 m	77.4	3.37 m	77.9
6′a	3.67 dd (12.0, 5.0)	62.7	3.67 dd (12.0, 5.0)	62.6	3.65 dd (12.0, 5.0)	62.5	3.65 dd (12.0, 5.0)	62.5
6′b	3.90 dd (12.0, 3.5)		3.89 dd (12.0, 3.0)		3.89 dd (12.0, 3.5)		3.89 dd (12.0, 3.0)	
1″		127.0		127.0		127.3		127.0
2″*cis*			7.35 d (2.0)	116.5	7.66 d (8.0)	133.4	7.73 d (8.0)	133.2
2″*trans*	7.21 d (1.8)	111.4	7.09 d (2.0)	114.1	7.47 d (8.0)	130.3	7.59 d (8.0)	130.8
3″*cis*		149.6	6.75 d (8.0)	148.1	6.76 d (8.0)	115.6	6.82 d (8.0)	116.0
3″*trans*					6.81 d (8.0)	116.6	6.96 d (8.0)	115.0
4″		151.8		151.7		161.0		159.5
5″*cis*			6.96 d (8.0)	111.7	6.76 d (8.0)	115.6	6.82 d (8.0)	116.0
5″*trans*	6.82 d (8.0)	116.2	6.94 d (8.0)	111.8	6.81 d (8.0)	116.6	6.96 d (8.0)	115.0
6″*cis*			7.13 dd (8.0, 2.0)	124.0	7.66 d (8.0)	133.4	7.73 d (8.0)	133.2
6″*trans*	7.10 dd (8.0, 1.8)	123.8	7.08 dd (8.0, 2.0)	123.8	7.47 d (8.0)	130.3	7.59 d (8.0)	130.8
*α*cis			5.83 d (12.0)	117.5	5.78 d (12.0)	116.2	5.85 d (12.0)	117.4
*α*trans	6.40 d (16.0)	115.6	6.36 d (16.0)	116.2	6.40 d (16.0)	116.0	6.36 d (16.0)	116.0
*β*cis			6.85 d (12.0)	144.5	6.90 d (12.0)	145.0	7.00 d (12.0)	144.2
*β*trans	7.64 d (16.0)	146.7	7.62 d (16.0)	146.2	7.65 d (16.0)	146.5	7.65 d (16.0)	146.3
C═O		168.9		168.7		168.8		168.9
OMe	3.90 s	56.1	3.88 s	56.0	3.88 s	56.0	3.88 s	56.0

[a] *J* values are in parentheses and reported in Hz; chemical shifts are given in ppm; assignments were confirmed by DQF-COSY, 1D-TOCSY, HSQC, and HMBC experiments.

regarding a single set of signals, consistent with the C2 symmetry of **1a**, whereas such kind of symmetry was lacking in **1b** (Figure 3). Thus, the structure of compound **1** was assigned as shown in Figure 1 and named argenteoside A.

The HRESIMS spectrum of **2** was identical with that of **1** (quasi-molecular peak at m/z 1039.3154 $[M + Na]^+$), thus indicating that these two compounds were isomers. The ^{1}H NMR spectra of **2** (Table 1) and **1** were very similar, except for proton signals of the cyclobutane ring appearing in **2** as two close

dx.doi.org/10.1021/jm301398y | J. Med. Chem. 2013, 56, 1583−1595

Table 3. ^{1}H and ^{13}C NMR Data of Compounds 16−19 (CD_3OD, 600 MHz)[a]

	16		17		18		19	
position	δ_H	δ_C	δ_H	δ_C	δ_H	δ_C	δ_H	δ_C
1	5.69 d (2.0)	93.9	4.97 d (9.0)	97.3	5.42 d (4.5)	93.3	5.25 d (5.5)	101.9
3a	5.31 d (2.5)	95.6	3.67 m	62.9	6.29 dd (6.0, 1.5)	141.1	3.66 m	57.3
3b			3.93 m				3.82 m	
4a	1.80 dd (14.0, 4.0)	34.4	1.59 br d (14.5)	23.5	5.06 dd (6.0, 3.5)	104.3	1.62 m	22.4
4b	2.49 m		1.85 m				1.72 m	
5	2.62 m	36.7	2.48 m	36.1	3.10 m	41.1	2.34 m	39.5
6	5.06 m	82.6	5.46 br d (9.5)	75.7	5.10 m	80.6	4.22 m	79.2
7a	2.21 dd (8.0, 4.0)	46.6	3.75 br s	58.7	1.90 br d (7.5)	42.2	2.00 br t (11.5)	45.8
7b	2.53 br t (8.0)				2.31 dd (15.0, 6.5)		2.40 dd (12.0, 6.0)	
8		80.6		66.4		82.7		85.0
9	2.69 br d (9.0)	51.1	2.40 dd (8.0, 1.5)	43.1	2.62 dd (6.5, 4.5)	51.1	2.26 dd (10.5, 5.5)	47.9
10a	3.46 d (13.0)	68.8	3.86 d (12.5)	66.4	3.58 d (12.0)	67.6	3.61 d (12.0)	78.3
10b	3.77 d (13.0)		4.13 d (12.5)		3.73 d (12.0)		3.81 d (12.0)	
Glc 1′	4.73 d (7.8)	98.6	4.74 d (7.8)	98.4	4.75 d (7.8)	99.4	4.38 d (7.8)	103.1
2′	3.21 dd (9.5, 7.8)	74.5	3.27 dd (9.0, 7.8)	74.7	3.28 dd (9.0, 7.8)	74.6	3.24 dd (9.0, 7.8)	74.4
3′	3.41 t (9.5)	77.9	3.44 t (9.0)	78.4	3.45 t (9.0)	77.6	3.42 t (9.0)	77.4
4′	3.32 t (9.5)	71.3	3.29 t (9.0)	71.8	3.46 t (9.0)	71.7	3.39 t (9.0)	71.7
5′	3.33 m	77.9	3.43 m	77.7	3.63 m	75.6	3.61 m	75.4
6′a	3.68 dd (12.0, 4.5)	62.6	3.67 dd (12.0, 5.0)	62.9	4.46 dd (12.0, 4.5)	64.3	4.34 dd (12.0, 5.0)	64.9
6′b	3.91 dd (12.0, 3.0)		3.93 dd (12.0, 3.0)		4.65 dd (12.0, 3.0)		4.68 dd (12.0, 3.0)	
1″		121.8		121.8		121.2		121.4
2″/6″	7.92 d (8.0)	132.5	7.93 d (8.0)	131.7	7.93 d (8.0)	132.7	7.92 d (8.0)	133.2
3″/5″	6.86 d (8.0)	116.2	6.88 d (8.0)	116.1	6.85 d (8.0)	115.6	6.86 d (8.0)	116.5
4″		164.3		164.1		164.0		164.2
C═O		167.4		167.8		167.6		167.6
1″						121.2		
2″/6″					7.93 d (8.0)	132.7		
3″/5″					6.83 d (8.0)	115.6		
4″						163.7		
C═O						167.6		

[a] J values are in parentheses and reported in Hz; chemical shifts are given in ppm; assignments were confirmed by DQF-COSY, 1D-TOCSY, HSQC, and HMBC experiments.

sets at δ 4.45 (1H, dd, J = 10.0, 9.0 Hz), 4.37 (1H, dd, J = 10.0, 9.0 Hz), 4.05 (1H, dd, J = 10.0, 9.0 Hz), and 3.97 (1H, dd, J = 10.0, 9.0 Hz). In the HSQC spectrum the methine protons signals showed correlations with the carbon signals at δ 41.8, 41.8, 48.0, and 48.3, respectively, confirming the presence of the cyclobutane ring. Also in this case the assignment was deduced from a combined analysis of 1D and 2D NMR experiments. The dimerization type of compound **2** was determined to be *head-to-tail* on the basis of the negative ion ESIMS/MS spectrum showing a major ion at m/z 507. The acid moiety of this dimer should possess the truxillic acid skeleton. Analysis of MS data indicated that compound **2** derives from a *head-to-tail* condensation, and it showed a different set of signals for the two halves of the molecule. Such observations indicated a structure without C2 symmetry, so excluding **2b** (Figure 2), and suggested stereoisomer **2a**, whose three-dimensional structure was in accordance with the crucial experimental NOE effect observed between H-7a and H-8a (Figure 3). Thus, the structure reported in Figure 1 was attributed to compound **2** named argenteoside B.

The molecular formula of compound **9** was assigned as $C_{25}H_{32}O_{13}$ by ESIMS (m/z 539 $[M - H]^-$) and ^{13}C NMR analyses. In the ESIMS/MS spectrum a peak at m/z 377 $[M - H\text{-}162]^-$ due to the loss of one hexose unit was observed. The ^{1}H NMR spectrum (Table 2) showed the presence of an iridoid glucoside. In addition, two vinylic protons of a *trans* double bond and three aromatic protons resolved as an ABX system were observed. These data and the presence of an aromatic methoxy singlet at δ 3.90 strongly suggested a ferulic acid moiety. HMBC correlations between H-7—C-6, H-9—C-6, H-6—CO, H-β—CO, H-β—C-2″, H-2″—C-4″, and H-5″—C-3″ substantiated the presence of an esterified hydroxy group at C-6, while the correlation between H-1′—C-1 confirmed the position of the glucopyranosyl moiety. The configuration of the sugar unit was assigned after hydrolysis of **9** with 1 N HCl and GC analysis of trimethylsilylated sugars by a chiral column. Therefore, the sugar unit was determined to be D-glucopyranose. The same procedure was also used to determine the absolute configuration of the sugar units of all new compounds. On the basis of this data, compound **9** was characterized to be 6-*O*-*trans*-feruloyl-5,7-bisdeoxycynanchoside.

Compounds **10**−**11** were assigned molecular formula $C_{25}H_{32}O_{13}$ (ESIMS at m/z 539 $[M - H]^-$), compounds **12** and **13**, $C_{24}H_{30}O_{12}$ (ESIMS at m/z 509 $[M - H]^-$), and compounds **14** and **15**, $C_{25}H_{32}O_{12}$ (ESIMS at m/z 523 $[M - H]^-$), respectively. Their structure was established by similar methods reported for the characterization of **9**. Compounds **10** and **11**, obtained as an inseparable mixture, were identified as 6-*O*-*cis*-isoferuloyl-5,7-bisdeoxycynanchoside (**10**) and 6-*O*-*trans*-isoferuloyl-5,7-bisdeoxycynanchoside (**11**); **12** and **13**, obtained as an inseparable mixture (**12** was also isolated as pure compound), were deduced to be 6-*O*-*cis*-*p*-coumaroyl-5,7-

dx.doi.org/10.1021/jm301398y | J. Med. Chem. 2013, 56, 1583−1595

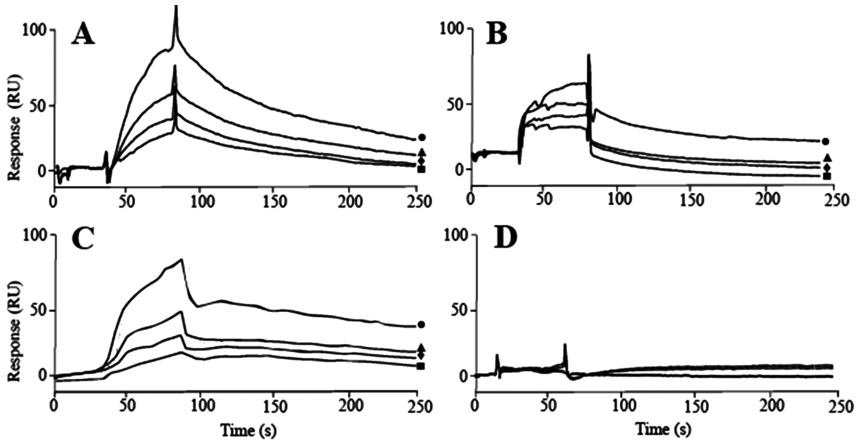

Figure 4. SPR results. Sensorgrams obtained by injecting four different concentrations (20 nM ■, 50 nM ◆, 250 nM ▲, and 1 μM ●) of compound **1** (A), **2** (B), radicicol (C), and **22** (D) on immobilized Hsp90 α.

bisdeoxycynanchoside (**12**) and 6-*O*-*trans*-*p*-coumaroyl-5,7-bisdeoxycynanchoside (**13**); **14** and **15**, obtained as an inseparable mixture, were defined as 6-*O*-*cis*-*p*-methoxycinnamoyl-5,7-bisdeoxycynanchoside (**14**) and 6-*O*-*trans*-*p*-methoxycinnamoyl-5,7-bisdeoxycynanchoside (**15**).

The molecular formula of compound **16** was determined by ESIMS and ^{13}C NMR to be $C_{22}H_{28}O_{12}$. The ESIMS of **16** showed a quasi-molecular ion peak at m/z 507 $[M + Na]^+$ and a peak at m/z 369 $[M + Na\text{-}138]^+$ due to the loss of a *p*-hydroxybenzoyl residue. The ^{13}C and ^{13}C DEPT NMR spectra (Table 3) of **16** displayed 22 signals, nine of which were assigned to the C_9-type iridoid aglycon moiety, while the remaining 13 signals corresponded to a hexose sugar residue and a *p*-hydroxybenzoyl group. The aglycon moiety of **16** was characterized as phelypaeside.[18] The acetal linkage between C-3 and C-10 was confirmed by HMBC correlations between H-10a,b (δ 3.46, 3.77) and C-3 (95.6 ppm). Moreover, the HMBC correlations between H-1 of glucose (δ 4.73) and C-1 (93.9 ppm), and H-6 (δ 5.06) and C═O (167.4 ppm), indicated that the glucose was attached to C-1 and the *p*-hydroxybenzoyl group to C-6 of the aglycon. Consequently, **16** was characterized as 6-*O*-*p*-hydroxybenzoylphelipaeside.

The ESIMS of **17** showed a quasi-molecular ion $[M - H]^-$ at m/z 483, consistent with a molecular formula of $C_{22}H_{28}O_{12}$. Comparison of its NMR spectra (Table 3) with those of catalposide (**3**)[14] showed that **17** differed in the signals due to the 3,4-olefinic moiety, replaced by two methylene groups. Therefore, **17** was identified as 3,4-dihydrocatalposide.

The molecular formula of **18**, $C_{29}H_{32}O_{14}$, was established by ESIMS and ^{13}C NMR. The NMR spectra of the iridoid moiety of **18** were superimposable on those of the known compound 6-*O*-*p*-hydroxybenzoyl-5,7-bisdeoxycynanchoside (**20**); however in the NMR spectra of **18**, an additional *p*-hydroxybenzoyl group was present. Its location at C-6_{glc} was suggested by the downfield shift of the signals due to H-$6a_{glc}$ and H-$6b_{glc}$ at δ 4.46 (1H, dd, J = 12.0, 4.5 Hz) and 4.65 (1H, dd, J = 12.0, 3.0 Hz), respectively. The above deduction was supported by the HMBC correlations between H-$6a_{glc}$ and H-$6b_{glc}$ and C═O at 167.6 ppm. Thus, **18** was identified as 6′-*O*-*p*-hydroxybenzoyl-6-*O*-*p*-hydroxybenzoyl-5,7-bisdeoxycynanchoside.

The ^{1}H and ^{13}C NMR spectra of compound **19** ($C_{22}H_{28}O_{11}$) (Table 3) displayed resonances due to a C_9-type iridoid with the absence of the characteristic olefinic proton signals. Thus, the aglycon of **19** was recognized to be *des*-*p*-hydroxybenzoyl-3-deoxycatalpin.[19] Signals of a β-glucopyranose and a *p*-hydroxybenzoyl residues were also evident. The chemical shift of H-6 suggested the presence of a substituent at C-6. From these data, the structure of **19** was determined as 6-*O*-(6′-*O*-*p*-hydroxybenzoyl)-β-D-glucopyranosyl-*des*-*p*-hydroxybenzoyl-3-deoxycatalpin.

Compounds **3**−**8** and **20**−**24** are known iridoids identified as catalposide (**3**),[14] specioside (**4**),[14] rehmaglutin A (**5**),[20] 6-*O*-(*p*-hydroxybenzoyl)-6-epiaucubin (**6**),[21] stereospermoside (**7**),[22] picroside II (**8**),[23] 6-*O*-*p*-hydroxybenzoyl-5,7-bisdeoxycynanchoside (**20**),[24] catalpin (**21**),[25] 3-methoxycatalpin (**22**),[26] 6-*O*-*trans*-feruloylcatalpol (**23**),[27] and *des*-*p*-hydroxybenzoyl-3-deoxycatalpin (**24**)[19] by comparison of their spectral ^{1}H and ^{13}C NMR and MS literature data.

Surface Plasmon Resonance Study. As a first step to study the ability of the iridoids to affect Hsp90 activity, a SPR based binding assay was performed. This analytic technique allows measuring kinetic and thermodynamic parameters of ligand−protein complex formation, and it is widely used to investigate several enzyme/inhibitor interactions.[12,28] Recently this approach was successfully applied to the study of the binding of small molecules to Hsp90.[13,29,30] In the present study, radicicol and 17-*N*-allylamino-17-demethoxygeldanamycin (17-AAG)[31,32] were used as positive controls. This assay allowed us to verify the affinity of iridoids **1**−**24** toward Hsp90 α, giving a detailed view of their interaction with the protein (Figure 4). Eleven of the tested compounds efficiently interacted with the immobilized protein, as demonstrated by the concentration-dependent responses, and by the clearly discernible exponential curves, during both the association and dissociation phases (Figure 4). The sensorgrams acquired for the compounds interacting with Hsp90 α were fitted to a single-site bimolecular interaction model (A + B = AB): using this approach, kinetic and thermodynamic parameters for each complex formation were achieved (Table 4). Compounds **1**−**4**, **17**, and **20** (Table 4) showed the higher affinity toward the chaperone, as inferred by the K_D values measured for the interaction of these compounds with Hsp90 α, ranging from 10 to 50 nM. However, argenteoside A (**1**) and B (**2**) showed a kinetic dissociation constant (k_d) notably lower than those measured for all the other tested compounds, thus indicating that the complexes formed by the interaction of the dimeric iridoids were extremely stable.

On the basis of the SPR data, some structure−activity relationship (SAR) evaluations can be attempted. Our screening

Table 4. Thermodynamic and Kinetic Constants Measured by SPR for the Interaction of Tested Compounds with Immobilized Hsp90 α

compound	K_D (nM)	k_d (1/s) × 10^3
1	14 ± 4	0.011 ± 0.001
2	50 ± 9	0.015 ± 0.004
3	12 ± 3	0.65 ± 0.08
4	26 ± 4	0.73 ± 0.12
5	2388 ± 152	163 ± 12
6	NB[a]	
7	NB	
8	NB	
9	NB	
10 + 11	NB	
12	73 ± 1	2.6 ± 0.4
12 + 13	NB	
14 + 15	NB	
16	NB	
17	16 ± 2	0.83 ± 0.07
18	139 ± 7	2.11 ± 0.8
19	NB	
20	31 ± 3	1.1 ± 0.1
21	5925 ± 317	208 ± 36
22	NB	
23	NB	
24	NB	
verminoside	348 ± 25	9.2 ± 0.8
secologanin	NB	
sweroside	NB	
adenosmoside	NB	
radicicol	4.2 ± 0.6	0.09 ± 0.01
17-AAG[b]	326 ± 28	6.3 ± 0.4

[a]NB: no binding observed in the SPR experiment for this compound. [b]17-*N*-Allylamino-17-demethoxygeldanamycin.

performed on secoiridoids, iridoids, and C_9-type iridoids demonstrated that only the latter were able to interact with Hsp90 α (verminoside versus secologanin, sweroside, adenosmoside). Comparison of the pseudothermodinamic dissociation constants for compounds **1**−**24** clearly showed that a *p*-hydroxybenzoyl moiety is critical for the Hsp90 α/iridoid interaction. Among the tested C_9-type iridoids, compounds **1**, **3**, and **17** showed the best K_D (Table 4), whereas compounds **4** and **12**, carrying a *p*-coumaroyl moiety, showed a moderate activity reduction. On the other hand, compound **8**, which differed in the presence of one additional methoxy group at the benzoyl residue, was inactive. The presence of the methoxy group at the benzoyl, cinnamoyl, and/or caffeoyl residues seems to reduce the activity (compound **4** and verminoside versus **9**−**11**, **14** + **15**, and **23**). The occurrence of an epoxide group at the iridoid portion increased the affinity toward the chaperone (**3** versus **20**). Different substituents at the aglycon moiety seem to have a negligible effect on the interaction between iridoids and Hsp90 α. The tricyclic nonglycosidic iridoids such as compounds **5**, **21**, **22**, and **24** showed fair or no activity. These findings suggested that the SAR for the C_9-type iridoids could involve complex relationships among multiple sites on the C_9-type backbone.

ATPase Assay. To study the possible inhibition of Hsp90 α by the iridoids and to compare the effects produced by monomeric and dimeric iridoids on the chaperone biological activity, the ATPase activity of the enzyme in the presence of compounds **1**−**4** was tested. Radicicol was selected as positive control, since this inhibitor interacts with the ATP binding site located in the *N*-terminus of the chaperone,[31] whereas as a negative control compound **22** was used. The results obtained (Figure 5) demonstrated that compounds **1**−**4** inhibit the

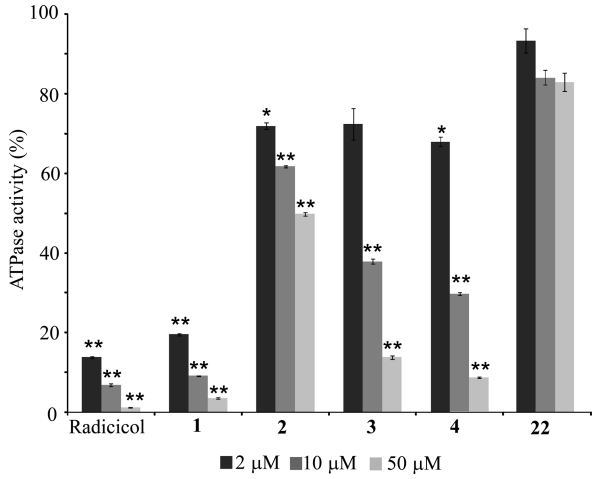

Figure 5. Inhibition of the ATPase activity of Hsp90 α by different concentration of compounds **1**−**4**. Radicicol and **22** were used as positive and negative controls, respectively. Data are the mean of two independent experiments performed in triplicate and were analyzed by *t* test (**22** vs testing compounds): $^*P < 0.05$, $^{**}P < 0.005$.

ATPase activity of Hsp90 α in a concentration-dependent manner, but these compounds clearly differed from each other in terms of inhibitory efficiency. Particularly, argenteoside A (**1**) was the most active and its potency was almost comparable to that measured for radicicol, whereas the other dimer (**2**) showed a weak inhibition potency. On the other hand, the two monomeric iridoids (**3** and **4**) showed very similar inhibition patterns. A comparison between ATPase activity inhibition and SPR data suggested that the different inhibitory efficiency shown by compounds **1**−**4** cannot be explained on the mere basis of their affinity toward Hsp90 α: even if comparable K_D were measured for the interaction of compounds **1** and **3** with Hsp90 α, the first showed a remarkably higher potency as an ATPase inhibitor.

Citrate Synthase Aggregation Assay. The high affinity and ATPase inhibitory efficiency shown by argenteoside A (**1**) prompted us to deepen the study of the interaction of this compound with Hsp90 α in order to rationalize the observed effects. Thus, the ability of compound **1** to inhibit the chaperone activity of Hsp90 α was evaluated by monitoring the citrate synthase (CS) thermal induced aggregation in the presence of Hsp90 α,[33] with or without this compound. Again, radicicol was used as a positive control (Figure 6). Upon incubation at elevated temperatures, CS underwent quantitative aggregation, but the presence of stoichiometric amounts of Hsp90 α changed significantly the aggregation kinetics. When a 4-fold molar excess of **1** was added to this mixture, the curve slope increased becoming almost comparable to that observed without the chaperone, confirming that this compound inhibited Hsp90 α chaperone activity. Notably, inhibition effects produced by **1** were comparable to those produced by radicicol under the same experimental conditions.

In Cell Studies. The antiproliferative activity of argenteoside A (**1**) was determined against solid cancer cell line HeLa (epithelial carcinoma), and it resulted in no cytotoxicity up to

dx.doi.org/10.1021/jm301398y | J. Med. Chem. 2013, 56, 1583−1595

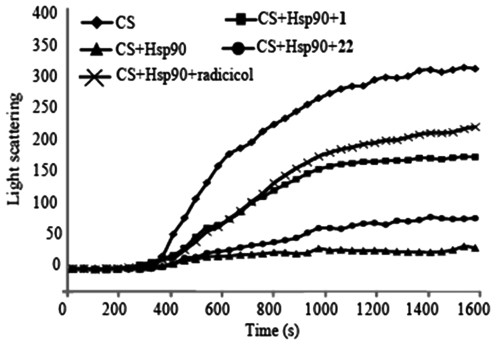

Figure 6. Aggregation kinetics of citrate synthase (CS) at 43 °C determined by light scattering. The spontaneous aggregation of CS at 43 °C (◆) and the aggregation of CS at 43 °C in the presence of 0.075 μM Hsp90 α and 0.3 μM ATP (▲), 0.075 μM Hsp90 α, 0.3 μM ATP and 0.3 μM **1** (■), or 0.075 μM Hsp90 α, 0.3 μM ATP and 0.3 μM **22** (●) are shown. Kinetics traces reported are the averages of two measurements.

100 μM. Compound **1** was tested for its effects on Hsp70, Hsp90 α, and Hsp90 client protein levels in HeLa cell line (Figure 7).

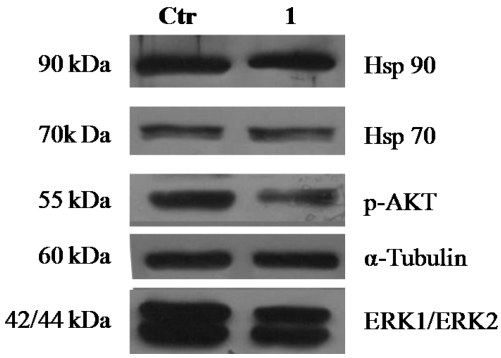

Figure 7. Effect of compound **1** on Hsp70, Hsp90, and on Hsp90 clients protein levels and HeLa cells. Protein levels were monitored using specific antibody, in equal amounts of total cellular extracts, obtained 24 h after treatment with different amounts of compound **1**. Tubulin was served as internal standard. Ctr = untreated cells.

Following 24 h exposure to 50 μM of **1**, the client protein *p*-AKT was strongly down-regulated, and a reduction of the ERK1/ERK2 level was also observed. Interestingly, cell exposure to **1** did not produce any enhancement of the Hsp70 level.

Study of Hsp90 α/1 Interaction. The achieved results demonstrated that argenteoside A (**1**) affects Hsp90 α activity both *in vitro* and into the cell. A limited proteolysis-mass spectrometry based strategy for the structural analysis of Hsp90 α/**1** complex, using trypsin and chymotrypsin as proteolytic probes, was used. This approach is based on the evidence that exposed, weakly structured, and flexible regions of a protein can be recognized by a proteolytic enzyme. Differences in the proteolytic patterns observed in the presence or in the absence of a putative protein ligand can be analyzed to identify the protein regions involved in the molecular interactions.[34] The efficiency of this approach in investigation of Hsp90/inhibitor complex was recently demonstrated.[13,29] A comparison between the cleavage sites observed on Hsp90 α and on Hsp90 α/**1** complex (Figure 8; Figure S1 and Table S1 in the Supporting Information) demonstrated that following its interaction with the iridoid the protein was protected from the hydrolysis at Tyr159, thus suggesting the *N*-terminal domain of Hsp90 α being involved in the molecule binding. Moreover, in the Hsp90 α/**1** complex

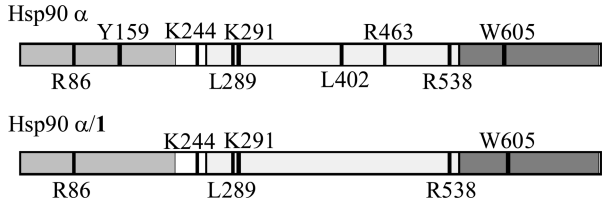

Figure 8. Schematic representation of the results obtained from limited proteolysis experiments (see Figure S1 and Table S1 in the Supporting Information). The preferential cleavage sites detected on recombinant Hsp90 α, and on the Hsp90 α/ **1** complex are in black. The Hsp90 α *N*-terminal domain is highlighted in light gray, the middle domain is boxed, and the *C*-terminal domain is highlighted in gray.

other two preferential cleavage sites located into the protein middle domain (Leu402 and Arg463) were masked from the enzymatic digestion. The involvement of Hsp90 α *N*-terminal domain in the binding of the dimeric compound **1** could account for the strong inhibitory effect on the Hsp90 α ATPase activity shown by this compound. Besides, the binding of **1** to the chaperone was also stabilized by some interactions involving protein middle domain; these interactions could enhance compound **1** anti-ATPase efficiency, since it is well reported how intra- and interdomain interactions cooperatively stabilize the active conformation of Hsp90 α ATPase active site.[35] Besides, since most of the client and cochaperones interact with the middle domain of Hsp90 α,[36,37] the binding of compound **1** could also mask residues playing a key role in the recognition of substrates enhancing the inhibitory effect of **1** toward the chaperone.

Molecular Modeling Analysis of Argenteoside A and B with Hsp90 α. On the basis of the above-mentioned results, we analyzed the interactions of argenteoside A (**1**) and B (**2**) with human Hsp90 α by means of molecular docking (Autodock4.2 software[38]). We used as a model receptor the X-ray structure of the *N*-terminal region disclosed by Huth et al.[39] in 2007 (pdb code: 2qg0). Prior to the docking calculations, we performed a conformational search on **1** and **2** by means of molecular dynamics (MD) using the Merck molecular force fields (MMFFs)[40] included in the Macro-Model software package.[41] On the resulting models, quantum mechanical (QM) optimization of the energies and geometries was performed in a vacuum at the DFT/mpw1pw91 level using 6-31g(d) as basis set (Gaussian 09 Software Package).[42] As reported,[43−45] the interactions with Asp93 and Thr184 played a major role in influencing Hsp90 α functionality guaranteeing, at least in theory, the ligand inhibitory character. In our proposed complex models relative to Hsp90 α/**1** and Hsp90 α/**2**, the fundamental contacts with these two amino acids were maintained. Interestingly, from the analysis of the docking results, it was possible to single out two different conformation families, accounting for two independent possible binding modes: (a) the first one regarded the family conformations where the phenolic portion of **1** and **2** interacted with Asp93 and Thr184 (Figure 9A,B), and (b) the second family included the docking poses showing interactions between the **1** and **2** sugar moieties and these two key aminoacids (Figure 9C,D). Considering the first group (Figure 9A,B), both **1** and **2** established hydrogen bonds between the iridoid phenolic moiety and the carboxylic group of Asp93 as H-bond donor, and the OH group of Thr184 as H-bond acceptor, and hydrophobic interactions with Ala55, Asn106, Asn51, and Lys58 (chain A) of Hsp90 α. However, the different condensation of **1** with respect to **2** (models **1a** and

dx.doi.org/10.1021/jm301398y | J. Med. Chem. 2013, 56, 1583−1595

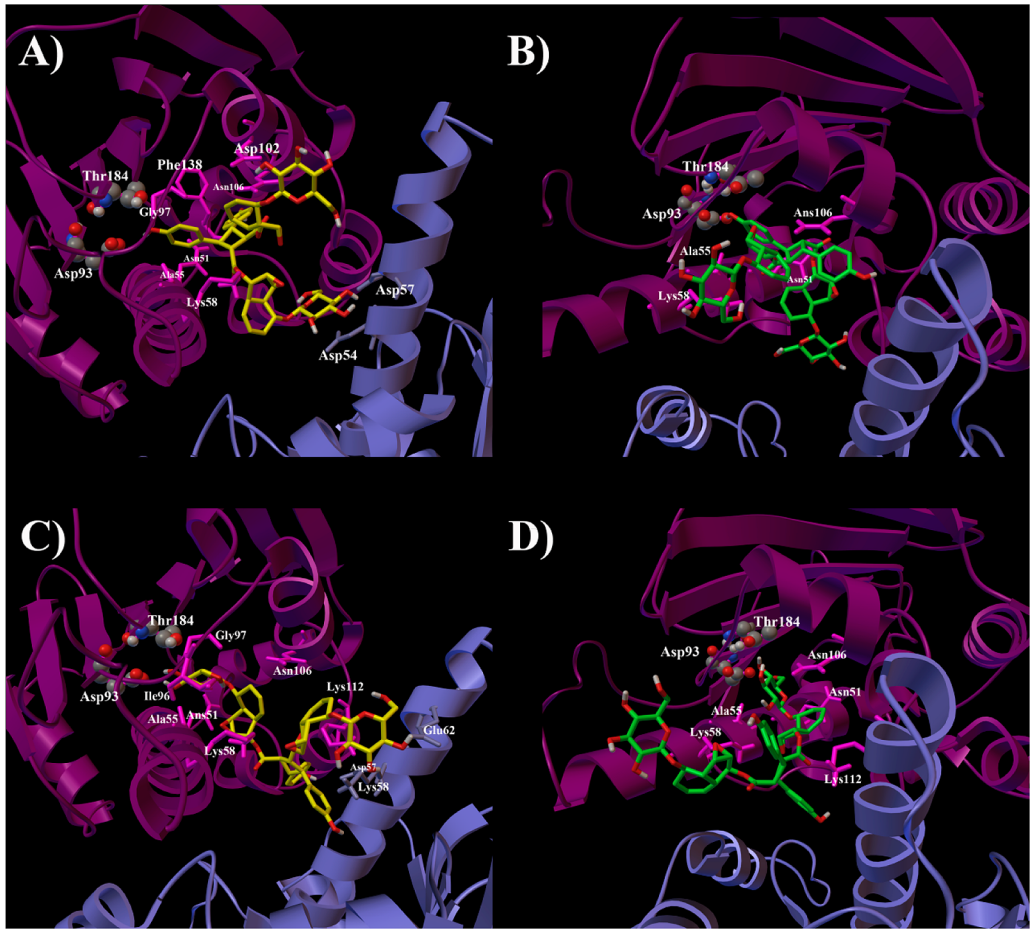

Figure 9. Two different spatial arrangements for argenteoside A (**1**, yellow) (A, C) and B (**2**, green) (B, D) in the binding site of *N*-terminal domain of Hsp90 α (crystal structure 2qg0). The protein was depicted by cpk (colored by atom type), purple (chain A) and light blue (chain B) ribbons, and sticks and balls.

2a in Figure 2) allowed further and specific contacts of **1** with both the Hsp90 α chains A and B: hydrophobic interactions with Asp102, Gly97, Phe138 (chain A), and Asp57 (chain B), and hydrogen bonds with Asp102, Asn106, Lys58 (chain A), and Asp54 (chain B). Moreover, considering the second family of docking poses (Figure 9C,D), in addition to the hydrogen bonds of the iridoids sugar moiety with Asp93 and Thr184, **1** and **2** established the same hydrophobic contacts with Ala55, Asn106, Asn51, Lys58, and Lys112 in the chain A (Figure 9C,D). Also in this case, the different condensation between the iridoids (**1a** and **2a** in Figure 2) allowed peculiar contacts of **1** with respect to **2** with the *N*-terminal region of Hsp90 α (Figure 9). In particular, **1** formed a hydrogen bond with Asn51, additional hydrophobic interactions with Gly97, Ile96 (chain A), Asp57, Glu62 (chain B), and a cation-π with Lys58 (chain B).

In summary, even if both dimers (**1** and **2**) were able to interact with the key aminoacids (Asp93 and Thr184), the different condensation mode, *head-to-head* or *head-to-tail* (**1a** and **2a** in Figure 2), caused a diverse spatial arrangement of **1** and **2** in the *N*-terminal domain (Figure 9), allowing additional interactions of **1** with respect to **2** with both the Hsp90 α chains. These further contacts likely accounted for the higher stability of Hsp90 α/**1** complex suggesting their critical role in the inhibition of the biological activity of the protein shown by these molecules.

The determination and evaluation of the affinity binding of small molecules, particularly natural compounds, to therapeutic targets are a significant component of drug discovery and lead optimization. SPR, limited proteolysis, molecular docking, and biochemical methods were used to study the interaction between argenteoside A (**1**) and full-length Hsp90 α. From our study, argenteoside A efficiently inhibited Hsp90 α ATPase activity, showing a very high affinity toward the protein. Besides, cell assays indicated that **1** treatment down-regulated Hsp90 α client proteins, without inducing any increase of Hsp70 levels. These results suggest argenteoside A as a good lead candidate compared with other Hsp90 inhibitors, also considering its low cytotoxicity. Moreover, C_9-type iridoids and particularly iridoid dimers may be considered new promising chemical scaffolds to develop new small molecules for the inhibition of Hsp90 α activity.

EXPERIMENTAL SECTION

Chemistry. Optical rotations were measured on a Perkin-Elmer 241 polarimeter equipped with a sodium lamp (589 nm) and a 1 dm microcell. UV spectra were recorded on a Perkin-Elmer-Lambda spectrophotometer. CD spectra were measured on a JASCO J-810 spectropolarimeter with a 0.1 cm cell in MeOH at room temperature with the following conditions: speed 50 nm/min, time constant 1 s, bandwidth 2.0 nm. NMR experiments were performed on a Bruker DRX-600 spectrometer at 300 K. 2D NMR spectra were acquired in CD_3OD in the phase-sensitive mode with the transmitter set at the solvent resonance and time proportional phase increment (TPPI) used to achieve frequency discrimination in the ω_1 dimension. The standard pulse sequence and phase cycling were used for DQF-COSY, TOCSY, HSQC, HMBC, and NOESY experiments. The NMR data were

dx.doi.org/10.1021/jm301398y | J. Med. Chem. 2013, 56, 1583−1595

processed on a Silicon Graphic Indigo2 Workstation using UXNMR software. HRESIMS data were acquired in the positive ion mode on a Q-TOF premier spectrometer equipped with a nanoelectrospray ion source (Waters-Milford, MA, USA). All the compounds met the criteria of ≥95% purity, as inferred by HPLC analyses performed using Agilent 1200 series systems with UV detection at 220 nm (Phenomenex Kinetex C_{18} 2.1 × 150 mm, 5 μm, 10−90% CH_3CN in H_2O with 0.1% TFA for 20 min at 0.5 mL/min). Column chromatography (CC) was performed over Sephadex LH-20. HPLC separations were conducted on a Shimadzu LC-8A series pumping system equipped with a Shimadzu RID-10A refractive index detector and Shimadzu injector on a C_{18} μ-Bondapak column (30 cm × 7.8 mm, 10 μm Waters, flow rate 2.0 mL/min).

Plant Materials. The leaves of *Tabebuia argentea* Britt. were collected in El Zoharia Research Garden of Cairo, Egypt, in May 2007. A voucher specimen (No. 7732 *Tabebuia argentea* /1) was deposited at the Herbarium Hortii Botanici Pisani, Pisa, Italy. The petioles of *Catalpa bignonioides* Walter were collected in Botanical Garden of Pisa, Italy, in October 2010.

Extraction and Isolation of the Iridoids. The leaves of *T. argentea* (750.0 g) were dried and extracted with solvents of increasing polarity, *n*-hexane, $CHCl_3$, $CHCl_3$-MeOH (9:1), and MeOH by exhaustive maceration (3 × 2 L), to give 10.9, 108.3, 8.3, and 40.3 g of the respective residues. The $CHCl_3$-MeOH extract (8.3 g) was separated by CC using Sephadex LH-20 (5 × 100 cm) with MeOH as eluent at a flow rate 0.8 mL/min. A total of 140 fractions were collected (10 mL each one). These were combined according to TLC analyses to give 10 pooled fractions (A-J). Fraction E (140.2 mg) was submitted to RP-HPLC eluting with MeOH-H_2O (45:55) to give compounds **6** (4.1 mg, t_R = 13 min) and **4** (3.5 mg, t_R = 25 min). The MeOH extract was partitioned between *n*-BuOH and H_2O. The *n*-BuOH soluble fraction (5.7 g) was separated by CC using Sephadex LH-20 (5 × 100 cm) with MeOH as eluent at a flow rate of 0.8 mL/min. A total of 195 fractions were collected (10 mL each one) and pooled into eight fractions (A-H). Fractions B (328.8 mg) and D (111.8 mg) were separately purified by RP-HPLC eluting with MeOH-H_2O (2:3) to give compounds **1** (3.1 mg, t_R = 24.1 min) and **2** (1.9 mg, t_R = 27.1 min), from fraction B, **5** (2.6 mg, t_R = 7.7 min), **7** (2.6 mg, t_R = 17.5 min), **3** (3.8 mg, t_R = 20.4 min), and **8** (2.1 mg, t_R = 21.3 min), from fraction D, respectively.

The petioles of *C. bignonioides* (70.0 g) were dried and extracted with solvents of increasing polarity, *n*-hexane, $CHCl_3$, $CHCl_3$-MeOH (9:1), and MeOH by exhaustive maceration (3 × 2 L), to give 0.5, 0.5, 2.0, and 2.9 g of the respective residues. The $CHCl_3$-MeOH extract (2.0 g) was separated by CC using Sephadex LH-20 (5 × 100 cm) with MeOH as eluent at a flow rate of 0.8 mL/min. A total of 56 fractions were collected (10 mL each one) and pooled in 11 fractions (A-I). Fraction C (472 mg) was subjected to HPCPC with $CHCl_3$-MeOH-H_2O-*n*-PrOH (9:12:8:1) in which the stationary phase consisted of the lower phase (ascending mode, flow rate 3 mL/min), with fractions of 3 mL collected. HPCPC fractions 31−42 (28 mg) and 48−55 (10 mg) were separately purified by RP-HPLC with MeOH-H_2O (2:3) to give pure compounds **24** (1.3 mg, t_R = 6 min) and **21** (1.2 mg, t_R = 14 min) from fractions 31−42 and compounds **14** (1.3 mg, t_R = 34 min) and **15** (1.5 mg, t_R = 36 min) from fractions 48−55. Fraction D (100 mg) was subjected to RP-HPLC with MeOH-H_2O (2:3) to yield pure compounds **22** (1.8 mg, t_R = 26 min) and **23** (1.6 mg, t_R = 36 min). Fraction E (350 mg) was subjected to HPCPC with $CHCl_3$-MeOH-H_2O-*n*-PrOH (9:12:8:1) in which the stationary phase consisted of the lower phase (ascending mode, flow rate 3 mL/min), with fractions of 3 mL collected. HPCPC fractions 33−38 (55 mg) and 42−44 (23 mg) were separately chromatographed by RP-HPLC with MeOH-H_2O (2:3) to afford pure compounds **20** (5.3 mg, t_R = 12 min), **16** (1.0 mg, t_R = 13 min), **12** (2.0 mg, t_R = 18 min), **13** (2.1 mg, t_R = 19 min) from fractions 33−38 and pure compounds **19** (1.0 mg, t_R = 11 min), **17** (1.8 mg, t_R = 12 min), **9** (1.4 mg, t_R = 16 min), **3** (4.3 mg, t_R = 18 min), **10** (1.6 mg, t_R = 21 min), and **11** (1.5 mg, t_R = 22 min), from fractions 42−44. The MeOH extract was partitioned between *n*-BuOH and H_2O, to afford a *n*-BuOH-soluble portion (820 mg). The *n*-BuOH residue was submitted to HPCPC with $CHCl_3$-MeOH-H_2O-*n*-PrOH (9:12:8:1) in which the stationary phase consisted of the lower phase (ascending mode, flow rate 3 mL/min), with fractions of 3 mL collected. HPCPC fraction 11 (51 mg) was chromatographed by RP-HPLC with MeOH-H_2O (2:3) to afford pure compounds **19** (1.2 mg, t_R = 11 min), **3** (5.0 mg, t_R = 18 min), and **18** (1.8 mg, t_R = 37 min).

*Compound (**1**).* Amorphous powder; $[\alpha]_D^{25}$ −24 (*c* 0.1, MeOH); UV (MeOH) λ_{max} (log ε) 235 (4.46), 280 (3.53) nm; ^1H and ^{13}C NMR (CD_3OD, 600 MHz); see Table 1; ESIMS: *m*/*z* 1039 $[M + Na]^+$, 1015 $[M - H]^-$, 803 $[M - H - 212]^-$, 507 $[M - H - 508]^-$, 211 $[M - H - 804]^-$, HRESIMS: *m*/*z* 1039.3186 $[M + Na]^+$ (calcd for $C_{48}H_{56}O_{24}$, 1016.3162).

*Compound (**2**).* Amorphous powder; $[\alpha]_D^{25}$-49 (*c* 0.1, MeOH); UV (MeOH) λ_{max} (log ε) 234 (4.09), 278 (3.73) nm; ^1H and ^{13}C NMR (CD_3OD, 600 MHz); see Table 1; ESIMS: *m*/*z* 1039 $[M + Na]^+$, 1015 $[M - H]^-$, 803 $[M - H - 508]^-$, HRESIMS: *m*/*z* 1039.3154 $[M + Na]^+$, (calcd for $C_{48}H_{56}O_{24}$, 1016.3162).

*6-O-trans-Feruloyl-5,7-bisdeoxycynanchoside (**9**).* $[\alpha]_D^{25}$-70 (*c* 0.1, MeOH); UV (MeOH) λ_{max} (log ε) 235 (4.03), 303 sh (3.78), 326 (3.98) nm; ^1H and ^{13}C NMR (CD_3OD, 600 MHz); see Table 2; ESIMS *m*/*z* 563 $[M + Na]^+$, 539 $[M - H]^-$, 377 $[M - H - 162]^-$, HRESIMS: *m*/*z* 563.1776 $[M + Na]^+$, (calcd for $C_{25}H_{32}O_{13}$, 540.1843).

*6-O-cis-Isoferuloyl-5,7-bisdeoxycynanchoside (**10**) and 6-O-trans-isoferuloyl-5,7-bisdeoxycynanchoside (**11**).* $[\alpha]_D^{25}$-58 (*c* 0.1, MeOH); UV (MeOH) λ_{max} (log ε) 240 (4.46), 295 sh (3.27), 327 (4.96) nm; ^1H and ^{13}C NMR (CD_3OD, 600 MHz); see Table 2; ESIMS *m*/*z* 563 $[M + Na]^+$, 383 $[M + Na - 180]^+$, 539 $[M - H]^-$, HRESIMS: *m*/*z* 563.1793 $[M + Na]^+$, (calcd for $C_{25}H_{32}O_{13}$, 540.1843).

*6-O-cis-p-Coumaroyl-5,7-bisdeoxycynanchoside (**12**) and 6-O-trans-p-coumaroyl-5,7-bisdeoxycynanchoside (**13**).* $[\alpha]_D^{25}$-77 (*c* 0.1, MeOH); UV (MeOH) λ_{max} (log ε) 230 (3.98), 313 (4.06) nm; ^1H and ^{13}C NMR (CD_3OD, 600 MHz); see Table 2; ESIMS *m*/*z* 533 $[M + Na]^+$, 371 $[M + Na - 162]^+$, 509 $[M - H]^-$, 347 $[M - H - 162]^-$, HRESIMS: *m*/*z* 533.1692 $[M + Na]^+$, (calcd for $C_{24}H_{30}O_{12}$, 510.1737).

*6-O-cis-p-Methoxycinnamoyl-5,7-bisdeoxycynanchoside (**14**) and 6-O-trans-p-methoxycinnamoyl-5,7-bisdeoxycynanchoside (**15**).* $[\alpha]_D^{25}$-54 (*c* 0.1, MeOH); UV (MeOH) λ_{max} (log ε) 225 (4.02), 309 (3.91) nm; ^1H and ^{13}C NMR (CD_3OD, 600 MHz); see Table 2; ESIMS *m*/*z* 547 $[M + Na]^+$, 523 $[M - H]^-$, HRESIMS: *m*/*z* 563.1799 $[M + Na]^+$, (calcd for $C_{25}H_{32}O_{12}$, 540.1843).

*6-O-p-Hydroxybenzoylphelipaeside (**16**).* $[\alpha]_D^{25}$-85 (*c* 0.1, MeOH); UV (MeOH) λ_{max} (log ε) 263 (3.67) nm; ^1H and ^{13}C NMR (CD_3OD, 600 MHz); see Table 3; ESIMS *m*/*z* 507 $[M + Na]^+$, 369 $[M + Na - 138]^+$, 483 $[M - H]^-$, 321 $[M - H - 162]^-$, HRESIMS: *m*/*z* 507.1502 $[M + Na]^+$, (calcd for $C_{22}H_{28}O_{12}$, 484.1581).

*3,4-Dihydrocatalposide (**17**).* $[\alpha]_D^{25}$-40 (*c* 0.1, MeOH); UV (MeOH) λ_{max} (log ε) 260 (4.03) nm; ^1H and ^{13}C NMR (CD_3OD, 600 MHz); see Table 3; ESIMS *m*/*z* 507 $[M + Na]^+$, 483 $[M - H]^-$, 321 $[M - H - 162]^-$, HRESIMS: *m*/*z* 507.1515 $[M + Na]^+$, (calcd for $C_{22}H_{28}O_{12}$, 484.1581).

*6′-O-p-Hydroxybenzoyl-6-O-p-hydroxybenzoyl-5,7-bisdeoxycynanchoside (**18**).* $[\alpha]_D^{25}$-63 (*c* 0.1, MeOH); UV (MeOH) λ_{max} (log ε) 258 (4.06), 320 sh (3.75) nm; ^1H and ^{13}C NMR (CD_3OD, 600 MHz); see Table 3; ESIMS *m*/*z* 627 $[M + Na]^+$, 489 $[M + Na - 138]^+$, 603 $[M - H]^-$, 465 $[M - H - 138]^-$, HRESIMS: *m*/*z* 627.1732 $[M + Na]^+$, (calcd for $C_{29}H_{32}O_{14}$, 604.1792).

*6-O-(6′-O-p-Hydroxybenzoyl)-β-D-glucopyranosyl-des-p-hydroxybenzoyl-3-deoxycatalpin (**19**).* $[\alpha]_D^{25}$-53 (*c* 0.1, MeOH); UV (MeOH) λ_{max} (log ε) 257 (4.02) nm; ^1H and ^{13}C NMR (CD_3OD, 600 MHz); see Table 3; ESIMS *m*/*z* 491 $[M + Na]^+$, HRESIMS: *m*/*z* 491.1560 $[M + Na]^+$, (calcd for $C_{22}H_{28}O_{11}$, 468.1632).

Acid Hydrolysis of Compounds 1−2 and 9−19. A solution of each compound (2.0 mg) in 1 N HCl (1 mL) was stirred at 80 °C in a stoppered reaction vial for 4 h. After cooling, the solution was evaporated under a stream of N_2. The residue was dissolved in 1-(trimethylsilyl)imidazole and pyridine (0.2 mL), and the solution was stirred at 60 °C for 5 min. After the solution was dried, the residue was partitioned between H_2O and $CHCl_3$. The $CHCl_3$ layer was analyzed by GC using a L-CP-Chirasil-Val column (0.32 mm × 25 m). Temperature of both the injector and detector was 200 °C. A temperature gradient system was used for the oven, starting at 100 °C for 1 min and increasing up to 180 °C at a rate of 5 °C/min. Peaks of the hydrolysate were detected by comparison with retention times of authentic samples of D-

glucose (Sigma Aldrich) after treatment with 1-(trimethylsilyl)-imidazole in pyridine.

Surface Plasmon Resonance Analyses. SPR analyses were performed as described elsewhere.[12] Briefly, SPR analyses were performed using a Biacore 3000 optical biosensor equipped with research-grade CM5 sensor chips (GE Healthcare). Using this platform, two separate recombinant Hsp90 surfaces, a BSA surface and an unmodified reference surface, were prepared for simultaneous analyses. Proteins (100 μg/mL in 10 mM sodium acetate, pH 5.0) were immobilized on individual sensor chip surfaces at a flow rate of 5 μL/min using standard amine-coupling protocols, to obtain densities of 8−12 kRU. Iridoids, as well as radicicol and 17-AAG were dissolved in 100% DMSO to obtain 4 mM solutions and diluted 1:200 (v/v) in PBS (10 mM NaH_2PO_4, 150 mM NaCl, pH 7.4) to a final DMSO concentration of 0.5%. Compounds were prepared as 2-fold dilutions into running buffer: for each sample, the complete binding study was performed using a six-point concentration series, typically spanning 0.025−1 μM, and triplicate aliquots of each compound concentration were dispensed into single-use vials. Included in each analysis were multiple blank samples of running buffer alone. Binding experiments were performed at 25 °C, using a flow rate of 50 μL/min, with 60 s monitoring of association and 200 s monitoring of dissociation. Simple interactions were adequately fit to a single-site bimolecular interaction model (A + B = AB), yielding a single K_D. Sensorgram elaborations were performed using the Biaevaluation software provided by GE Healthcare.

ATP Hydrolysis Inhibition. The Discover RX ADP HunterTM Plus Assay kit was used following the manufacturer's instructions. ATPase reactions were carried out for 60 min at 40 °C in 100 mM Tris pH 7.4, 100 μM ATP, and 40 nM Hsp90 α in the presence of different concentrations of compounds **1**−**4**, **22**, or radicicol. ADP generation was measured using a Perkin-Elmer LS 55 fluorimeter (540 nm excitation and 620 nm emission). Fluorescence intensity values measured for Hsp90 α without any testing compound was assumed as 100% of enzyme activity. The background reaction rate was measured in a reaction lacking enzyme or substrate and subtracted from the experimental rates.

Citrate Synthase Aggregation Assay,. Chaperone activity was evaluated as reported elsewhere by monitoring the thermal-induced aggregation of CS (0.075 μM) in the absence or in the presence of a stoichiometric amount of Hsp90 α and 0.3 μM ATP, and with or without a 4-fold molar excess of **1**, **22**, or radicicol. Aggregation was initiated by unfolding CS incubating the protein in 40 mM HEPES−KOH, pH 7.5 at 43 °C. Aggregation was monitored by measuring light scattering at right angles with a Perkin-Elmer LS 55 fluorimeter in stirred and thermostatted quartz cells. Both the emission and excitation wavelengths were set at 500 nm, and the band-pass was 2 nm. Kinetics traces reported here are the averages of two measurements.

Statistical Analysis. All the reported values represent the mean ± standard deviation (SD) of at least two independent experiments performed in triplicate. Where necessary, data were statistically compared by *t*-test.

Cell Culture and Treatment. HeLa (epithelial carcinoma) cells, obtained from Cell Bank in GMP-IST (Genova, Italy), were maintained in RPMI 1640 medium or Dulbecco's modified Eagle medium (DMEM), respectively, supplemented with 10% (v/v) FBS, 2 mM L-glutamine and antibiotics (100 U/mL penicillin, 100 μg/mL streptomycin) purchased from Invitrogen (Carslbad, CA, USA), at 37 °C in humidified atmosphere with 5% CO_2. To ensure logarithmic growth, cells were subcultured every 2 days. Stock solution 50 mM of compound **1** in DMSO was stored at −20 °C in the dark and diluted just before using in the sterile culture medium. In all the experiments, final concentration of DMSO did not exceed 0.15% (v/v).

Cell Proliferation and Viability. HeLa (5000/well) cells were seeded in triplicate in 96-well plates and incubated for 24 h in the absence and in the presence of compound **1** (at a concentration between 100 μM and 0.5 μM). The number of viable cells was quantified by using a [3-4,5-dimethyldiazol-2-yl]-2,5-diphenyl tetrazolium bromide (MTT, Sigma-Aldrich) conversion assay according to the method of Mosmann.[46] Briefly, after the indicate treatment, 25 μL of MTT (5 mg/mL in PBS) was added and was incubated for an additional 3 h at 37 °C. Thereafter, cells were lysed and solubilized with 100 μL of buffer containing 50% (v/v) *N*,*N*-dimethylformamide, 20% SDS, with an adjusted pH 4.5. The absorbance was measured with a microplate reader (Titertek multiskan MCC7340, LabSystems, Vienna, VA, USA) equipped with a 620 nm filter. IC_{50} values were calculated from cell viability dose−response curves and defined as the concentration resulting in 50% inhibition of cell survival at 24 h, compared to untreated cells.

Western Blot Analysis. Treated cells were harvested and disrupted by freeze−thawing in RIPA buffer (50 mM Hepes, 10 mM EDTA, 150 mM NaCl, 1% NP-40, 0.5% sodium deoxycholate, 0.1% SDS, pH 7.4) supplemented with protease inhibitors cockatil (Sigma-Aldrich). Cell debris was removed by centrifugation at 4 °C, and the protein concentration in the resulting supernatants was determined according to a Bio-Rad Protein assay (Biorad Laboratories, CA, USA). Clarified cell lysate (30 ug) were subjected to SDS-PAGE under denatured reducing conditions. Percentage of polyacrylamide was chosen based on the molecular weight of protein to be detected. Proteins were then transferred to nitrocellulose membranes and were blocked for 3 h with 3% BSA in 50 mM Tris, 200 mM NaCl, 0.1% Tween 20, before being incubated at 4 °C overnight with the desired primary antibodies diluted 1:1000. After washing, the membranes were incubated at room temperature (1 h) with an appropriate peroxidase-conjugate secondary antibodies. Immunoreactive protein bands were detected by enhanced chemiluminescence reagent (ECL) according the manufacturer's instructions.

Limited Proteolysis. Limited proteolysis experiments were performed on recombinant Hsp90 α at 37 °C, PBS 0.1% DMSO, using trypsin or chymotrypsin as the proteolytic agent; 30 μL of a 3 μM Hsp90 α solution was used for each experiment. Binary complex Hsp90 α/**1** was formed by incubating the protein with a 5:1 molar excess of the inhibitor at 37 °C for 15 min prior to proteolytic enzyme addition. Isolated protein and complex were digested using a 1:100 (w/w) enzyme to substrate ratio. The extent of the reactions was monitored on a time-course basis by sampling the incubation mixture after 5, 15, and 30 min of digestion. Samples were analyzed by MALDITOF/MS using a MALDI micro MX (Waters). Mass data were elaborated using the Masslynx software (Waters). Preferential hydrolysis sites on Hsp90 α under different conditions were identified on the basis of the fragments released during the enzymatic digestions.

Computational Details. Molecular Dynamics calculations of **1** and **2** were performed with the Macromodel 8.5 software package[41] using the MMFFs[40] force field. All the structures were minimized by using a Polak−Ribiere Conjugate Gradient (PRCG, 50 000 steps, maximum derivative <0.005 kcal/mol). We then optimized in a vacuum the energies and geometry of iridoids by QM at the DFT/mpw1pw91 level using 6-31g(d) as basis set (Gaussian 09 Software Package).[42] The so-obtained iridoids geometries were used for molecular docking calculations by Autodock 4.2 software.[38] All calculations were performed on 4 x AMD Opteron 16 Core at 2.3 GHz, using a grid box size of 76 × 88 × 126 for Hsp90 α (pdb code: 2qg0)[39] with spacing of 0.375 Å between the grid points and centered at 19.709 (x), 25.167 (y), 16.15 (z), covering the *N*-terminal domain. For all the docked structures, all bonds were treated as active torsional bonds except the bonds in cycles, which were considered fixed together with the receptor. To achieve a representative conformational space during the docking studies and for taking into account the variable number of active torsions, 10 calculations consisting of 256 runs were performed, obtaining 2560 structures for each ligand. The Lamarckian genetic algorithm (LGA) was employed for docking experiments, choosing an initial population of 600 randomly placed individuals. The maximum number of energy evaluations and of generations was set up to 5×10^6 and to 6×10^6 respectively. Results that differed by <3.5 Å in positional root-mean-square deviation (RMSD) were clustered together and represented by the most favorable free energy of binding. Illustrations of the 3D models were generated with the Python software[47] using MGLTools 1.5.6.

■ ASSOCIATED CONTENT

Supporting Information

Limited proteolysis data. This material is available free of charge via the Internet at http://pubs.acs.org.

■ AUTHOR INFORMATION

Corresponding Author

*Phone: +39-089-969754. Fax: +39-089-969602. E-mail: detommasi@unisa.it.

Notes

The authors declare no competing financial interest.

■ ACKNOWLEDGMENTS

Authors would like to thank Dr. Maryan Bruzual De Abreu and Dr. Lorenzo Picchi for their help in the iridoids isolation. This work was financed by the University of Salerno and by Ministero dell'Istruzione, dell'Università e della Ricerca (MIUR), PRIN 2009 "Design, conformational and configurational analysis of novel molecular platforms" and PRIN 2008 "Studio chimico di estratti vegetali ad attività antimicrobica ed antiinfiammatoria".

■ ABBREVIATIONS USED

CC, column chromatography; CS, citrate synthase; 1D-TOCSY, monodimensional total correlation spectroscopy; DQF-COSY, double quantum filtered correlation spectroscopy; Hsp90, heat shock protein 90; HSQC, heteronuclear single quantum coherence; HMBC, heteronuclear multibond correlation spectroscopy; LGA, Lamarckian genetic algorithm; MD, molecular dynamics; MMFFs, Merck molecular force fields; NOE, nuclear overhauser effect; *p*-AKT, phosphorylated protein kinase AKT; QM, quantum mechanical; SAR, structure−activity relationship; SPR, surface plasmon resonance

■ REFERENCES

(1) Pratt, W. B.; Toft, D. O. Regulation of signaling protein function andtrafficking by the hsp90/hsp70-based chaperone machinery. *Exp. Biol. Med.* **2003**, *228*, 111−133.

(2) Zhang, H.; Burrows, F. Targeting multiple signal transduction pathways through inhibition of Hsp90. *J. Mol. Med.* **2004**, *82*, 488−499.

(3) Didelot, C.; Lanneau, D.; Brunet, M.; Joly, A. L.; De Thonel, A.; Chiosis, G.; Garrido, C. Anti-cancer therapeutic approaches based on intracellular and extracellular heat shock proteins. *Curr. Med. Chem.* **2007**, *14*, 2839−2847.

(4) Calderwood, S. K.; Khaleque, M. A.; Sawyer, D. B.; Ciocca, D. R. Heat shock proteins in cancer: chaperones of tumorigenesis. *Trends Biochem. Sci.* **2006**, *31*, 164−172.

(5) Beck, R.; Verrax, J.; Gonze, T.; Zappone, M.; Pedrosa, R. C.; Taper, H.; Feron, O.; Calderon, P. B. Hsp90 cleavage by an oxidative stress leads to its client proteins degradation and cancer cell death. *Biochem. Pharmacol.* **2009**, *77*, 375−383.

(6) Hagn, F.; Lagleder, S.; Retzlaff, M.; Rohrberg, J.; Demmer, O.; Richter, K.; Buchner, J.; Kessler, H. Structural analysis of the interaction between Hsp90 and the tumor suppressor protein p53. *Nat. Struct. Mol. Biol.* **2011**, *18*, 1086−1093.

(7) Crawford, L. J.; Walker, B.; Irvine, A. E. Proteasome inhibitors in cancer therapy. *J. Cell Commun. Signal* **2011**, *5*, 101−110.

(8) Modi, S.; Stopeck, A.; Linden, H.; Solit, D.; Chandarlapaty, S.; Rosen, N.; D'Andrea, G.; Dickler, M.; Moynahan, M. E.; Sugarman, S.; Ma, W.; Patil, S.; Norton, L.; Hannah, A. L.; Hudis, C. HSP90 inhibition is effective in breast cancer: a phase II trial of tanespimycin (17-AAG) plus trastuzumab in patients with HER2-positive metastatic breast cancer progressing on trastuzumab. *Clin. Cancer Res.* **2011**, *17*, 5132−5139.

(9) Yao, Q.; Weigel, B.; Kersey, J. Synergism between etoposide and 17-AAG in leukemia cells: critical roles for Hsp90, FLT3, topoisomerase II, Chk1, and Rad51. *Clin. Cancer Res.* **2007**, *13*, 1591−1600.

(10) Davenport, J.; Manjarrez, J. R.; Peterson, L.; Krumm, B.; Blagg, B. S. J.; Matts, R. L. Gambogic acid, a natural product inhibitor of Hsp 90. *J. Nat. Prod.* **2011**, *74*, 1085−1092.

(11) Hung, M.-S.; Xu, Z.; Lin, Y.-C.; Mao, J.-H.; Yang, C. T.; Chang, P.-J.; Jablons, D. M.; You, L. Identification of hematein as a novel inhibitor of protein kinase CK2 from a natural product library. *BMC Cancer* **2009**, *9*, 135.

(12) Dal Piaz, F.; Vassallo, A.; Lepore, L.; Tosco, A.; Bader, A.; De Tommasi, N. Sesterterpenes as tubulin tyrosine ligase inhibitors. First insight of structure-activity relationships and discovery of new lead. *J. Med. Chem.* **2009**, *52*, 3814−3828.

(13) Dal Piaz, F.; Malafronte, N.; Romano, A.; Gallotta, D.; Belisario, M. A.; Bifulco, G.; Gualtieri, M. J.; Sanogo, R.; De Tommasi, N.; Pisano, C. Structural characterization of tetranortriterpenes from *Pseudrocedrela kotschyi* and *Trichilia emetica* and study of their activity towards the chaperone Hsp90. *Phytochemistry* **2012**, *75*, 78−89.

(14) El Naggar, S. F.; Doskotch, R. W. Specioside: A new iridoid glycoside from *Catalpa speciosa*. *J. Nat. Prod.* **1980**, *43*, 524−526.

(15) Hartley, R. D.; Morrison, W. H., III; Balza, F.; Towers, G. H. N. Substituted truxillic and truxinic acids in cell walls of *Cynodon dactylon*. *Phytochemistry* **1990**, *29*, 3699−3703.

(16) Sudo, H.; Ide, T.; Otsuka, H.; Hirata, E.; Takushi, A.; Shinzato, T.; Takeda, Y. Megastigmane, benzyl and phenethyl alcohol glycosides, and 4,4-dimethoxy-*β*-truxinic acid catalpol diester from the leaves of *Premna subscandens* MERR. *Chem. Pharm. Bull.* **2000**, *48*, 542−546.

(17) Stewart, D.; Robertson, G. W.; Morrison, I. M. Identification of cyclobutane-type dimers of substituted cinnamic acids by gas chromatography/mass spectrometry. *Rapid Commun. Mass Spectrom.* **1992**, *6*, 46−53.

(18) Deyama, T.; Yahikozawa, K.; Al-Easa, H. S.; Rizk, A. M. Constituents of plants growing in Qatar: Part XXX. A new iridoid from *Cistanche phelypaea* (L.) Cout. *Intern. J. Chem.* **1995**, *6*, 107−112.

(19) Machida, K.; Ikeda, C.; Kakuda, R.; Yaoita, Y.; Kikuchi, M. Studies on the constituents of *Catalpa* species V. Iridoids from Catalpa fructus. *Nat. Med.* **2001**, *55*, 61−63.

(20) Morota, T.; Nishimura, H.; Sasaki, H.; Chin, M.; Sugama, K.; Katsuhara, T.; Mitsuhashi, H. Five cyclopentanoid monoterpenes from *Rehmannia glutinosa*. *Phytochemistry* **1989**, *28*, 2385−2391.

(21) Bianco, A.; Passacantilli, P.; Nicoletti, M. Alves de Lima, R. Iridoids in equatorial and tropical flora. V. A new glucosidic iridoid from *Tecoma chrysantha* Jacq. *Gazz. Chim. Ital.* **1982**, *112*, 227−229.

(22) Kanchanapoom, T.; Noiarsa, P.; Otsuka, H.; Ruchirawat, S. Lignan, phenolic and iridoid glycosides from *Stereospermum cylindricum*. *Phytochemistry* **2006**, *67*, 516−520.

(23) Laurie, W. A.; McHale, D.; Sheridan, J. B. A cucurbitacin glycoside from *Picrorhiza kurrooa*. *Phytochemistry* **1985**, *24*, 2659−2661.

(24) Iwagawa, T.; Hamada, T.; Kurogi, S.; Hase, T.; Okubo, T.; Kim, M. Iridoids from *Catalpa bignonioides*. *Phytochemistry* **1991**, *30*, 4057−4060.

(25) Nozaka, T.; Watanabe, F.; Ishino, M.; Morimoto, I.; Kondoh, H.; Koyama, K.; Natori, S. A mutagenic new iridoid in the water extract of Catalpae fructus. *Chem. Pharm. Bull.* **1989**, *37*, 2838−2840.

(26) Kanai, E.; Machida, K.; Kikuchi, M. Studies on the constituents of *Catalpa* species. I. Iridoids from Catalpae fructus. *Chem. Pharm. Bull.* **1996**, *44*, 1607−1609.

(27) Stuppner, H.; Wagner, H. Minor iridoid and phenol glycosides of *Picrorhiza kurrooa*. *Planta Med.* **1989**, *55*, 467−469.

(28) Cooper, M. A. Label-free screening of bio-molecular interactions. *Anal. Bioanal. Chem.* **2003**, *377*, 834−842.

(29) Giommarelli, C.; Zuco, V.; Favini, E.; Pisano, C.; Dal Piaz, F.; De Tommasi, N.; Zunino, F. The enhancement of antiproliferative and proapoptotic activity of HDAC inhibitors by curcumin is mediated by Hsp90 inhibition. *Cell. Mol. Life Sci.* **2010**, *67*, 995−1004.

(30) Dal Piaz, F.; Vassallo, A.; Chini, M. G.; Cordero, F. M.; Cardona, F.; Pisano, C.; Bifulco, G.; De Tommasi, N.; Brandi, A. Natural

iminosugar (+)-lentiginosine inhibits ATPase and chaperone activity of Hsp90. *PLoS One* **2012**, *7*, e43316.
(31) Schulte, T. W.; Akinaga, S.; Soga, S.; Sullivan, W.; Stensgard, B.; Toft, D.; Neckers, L. M. Antibiotic radicicol binds to the *N*-terminal domain of Hsp90 and shares important biologic activities with geldanamycin. *Cell Stress. Chaperon* **1998**, *3*, 100−108.
(32) Guo, W.; Reigan, P.; Siegel, D.; Zirrolli, J.; Gustafson, D.; Ross, D. Formation of 17-allylamino-demethoxygeldanamycin (17-AAG) hydroquinone by NAD(P)H:quinone oxidoreductase 1: role of 17-AAG hydroquinone in Heat Shock Protein 90 inhibition. *Cancer Res.* **2005**, *65*, 10006−10015.
(33) Jakob, U.; Lilie, H.; Meyer, I.; Buchner, J. Transient interaction of Hsp90 with early unfolding intermediates of citrate synthase. *J. Biol. Chem.* **1995**, *270*, 7288−7294.
(34) Casbarra, A.; Birolo, L.; Infusini, G.; Dal Piaz, F.; Svensson, M.; Pucci, P.; Svanborg, C.; Marino, G. Conformational analysis of HAMLET, the folding variant of human α-lactalbumin associated with apoptosis. *Protein Sci.* **2004**, *13*, 1322−1330.
(35) Cunningham, C. N.; Krukenberg, K. A.; Agard, D. A. Intra- and intermonomer interactions are required to synergistically facilitate ATP hydrolysis in Hsp90. *J. Biol. Chem.* **2008**, *283*, 21170−21178.
(36) Ji-Sook, H. The Hsp90 chaperone machinery: from structure to drug development. *BMB Rep.* **2009**, *42*, 623−630.
(37) Meyer, P.; Prodromou, C.; Hu, B.; Vaughan, C.; Roe, S. M.; Panaretou, B.; Piper, P. W.; Pearl, L. H. Structural and functional analysis of the middle segment of Hsp90: implications for ATP hydrolysis and client protein and cochaperone interactions. *Mol. Cell* **2003**, *11*, 647−658.
(38) Morris, G. M.; Huey, R.; Lindstrom, W.; Sanner, M. F.; Belew, R. K.; Goodsell, D. S.; Olson, A. J. AutoDock4 and AutoDockTools4: automated docking with selective receptor flexibility. *J. Comput. Chem.* **2009**, *30*, 2785−2791.
(39) Huth, J. R.; Park, C.; Petros, A. M.; Kunzer, A. R.; Wendt, M. D.; Wang, X.; Lynch, C. L.; Mack, J. C.; Swift, K. M.; Judge, R. A.; Chen, J.; Richardson, P. L.; Jin, S.; Tahir, S. K.; Matayoshi, E. D.; Dorwin, S. A.; Ladror, U. S.; Severin, J. M.; Walter, K. A.; Bartley, D. M.; Fesik, S. W.; Elmore, S. W.; Hajduk, P. J. Discovery and design of novel HSP90 inhibitors using multiple fragment-based design strategies. *Chem. Biol. Drug. Des.* **2007**, *70*, 1−12.
(40) Halgren, T. A.; MMFF, V. I. MMFF94s option for energy minimization studies. *J. Comput. Chem.* **1999**, *20*, 720−729.
(41) (a) Mohamadi, F.; Richards, N. G. J.; Guida, W. C.; Liskamp, R.; Lipton, M.; Caufield, C.; Chang, G.; Hendrickson, T.; Still, W. C. MacroModel − an integrated software system for modeling organic and bioorganic molecules using molecular mechanics. *J. Comput. Chem.* **1990**, *11*, 440−467. (b) *MacroModel*, Version 8.5; Schrödinger LLC: New York, 2003.
(42) Frisch, M. J.; Trucks, G. W.; Schlegel, H. B.; Scuseria, G. E.; Robb, M. A.; Cheeseman, J. R.; Scalmani, G.; Barone, V.; Mennucci, B.; Petersson, G. A.; Nakatsuji, H.; Caricato, M.; Li, X.; Hratchian, H. P.; Izmaylov, A. F.; Bloino, J.; Zheng, G.; Sonnenberg, J. L.; Hada, M.; Ehara, M.; Toyota, K.; Fukuda, R.; Hasegawa, J.; Ishida, M.; Nakajima, T.; Honda, Y.; Kitao, O.; Nakai, H.; Vreven, T.; Montgomery, J. A., Jr.; Peralta, J. E.; Ogliaro, F.; Bearpark, M.; Heyd, J. J.; Brothers, E.; Kudin, K. N.; Staroverov, V. N.; Kobayashi, R.; Normand, J.; Raghavachari, K.; Rendell, A.; Burant, J. C.; Iyengar, S. S.; Tomasi, J.; Cossi, M.; Rega, N.; Millam, J. M.; Klene, M.; Knox, J. E.; Cross, J. B.; Bakken, V.; Adamo, C.; Jaramillo, J.; Gomperts, R.; Stratmann, R. E.; Yazyev, O.; Austin, A. J.; Cammi, R.; Pomelli, C.; Ochterski, J. W.; Martin, R. L.; Morokuma, K.; Zakrzewski, V. G.; Voth, G. A.; Salvador, P.; Dannenberg, J. J.; Dapprich, S.; Daniels, A. D.; Farkas, O.; Foresman, J. B.; Ortiz, J. V.; Cioslowski, J.; Fox, D. J. *Gaussian 09*, Revision A.02; Gaussian, Inc.: Wallingford, CT, 2009.
(43) Sugunadevi, S.; Sundarapandian, T.; Shalini, J.; Keun, W. L. Pharmacophore based virtual screening, molecular docking studies to design potent heat shock protein 90 inhibitors. *Eur. J. Med. Chem.* **2011**, *46*, 2937−2947.
(44) Stebbins, C. E.; Russo, A. A.; Schneider, C.; Rosen, N.; Hartl, F. U.; Pavletich, N. P. Crystal structure of an Hsp90−geldanamycin complex: targeting of a protein chaperone by an antitumor agent. *Cell* **1997**, *89*, 239−250.
(45) Obermann, W. M. J.; Sondermann, H.; Russo, A. A.; Pavletich, N. P.; Hartl, U. H. In vivo function of Hsp90 is dependent on ATP binding and ATP hydrolysis. *J. Cell. Biol.* **1998**, *143*, 901−910.
(46) Mosmann, T. Rapid colorimetric assay for cellular growth and survival: application to proliferation and cytotoxicity assays. *J. Immunol. Methods* **1983**, *65*, 55−63.
(47) Sanner, M. F. A programming language for software integration and development. *J. Mol. Graphics* **1999**, *17*, 57−61.